Int. J. Electrochem. Sci., 13 **(2018)** 275 – 286, doi: 10.20964/2018.01.04

International Journal of
ELECTROCHEMICAL
SCIENCE
www.electrochemsci.org

Ultrasonic Synthesis of α-MoO_3 Nanobelt@CNTs Composite for Lithium Battery and its Electrochemical Performances

Wanzheng Lu[1], *Xiaolan Chen*[1], *Mingzhe Xue*[1*], *Yongli Cui*[2], *Quanchao Zhuang*[2]

[1] Clean Energy Automotive Engineering Center, School of Automobile Studies, Tongji University, Shanghai 201804, P. R. China;
[2] School of Materials Science and Engineering, China University of Mining and Technology, Xuzhou, Jiangsu 221116, P. R. China.
[*]E-mail: mzxue@tongji.edu.cn

Received: 16 September 2017 / *Accepted:* 19 October 2017 / *Online Published:* 1 December 2017

α-MoO_3 nanobelt@CNTs composite is synthesized from α-MoO_3 nanobelt and multi-walled carbon nanotubes (CNTs) via ultrasonic mixing process. XRD and SEM measurement prove the layer structure and nano-belt morphology of the product. Although α-MoO_3 nanobelt@CNTs composite delivers less initial discharge capacity than pure α-MoO_3 nanobelt, cycling performance is improved due to the introduction of CNTs into composite. Microscopic mechanism of Li^+ transportation through α-MoO_3 nanobelt@CNTs composite electrode is revealed by cyclic voltammetry (CV) and electrochemical impedance spectroscopy (EIS). Nyquist plots of α-MoO_3 nanobelts@CNTs composite electrode *vs.* polarization potentials in the first discharge process shows that during Li^+ intercalates into α-MoO_3 nanobelts@CNTs composite electrode, SEI-film resistance (R_{SEI}), electronic transmission resistance (R_e), and charge transfer resistance (R_{ct}) play an important role in different periods (2.9-2.0 V, 2.0-1.5 V and 1.4-1.2 V), respectively.

Keywords: α-MoO_3 nanobelt@CNTs composite; ultrasonic synthesis; microscopic mechanism; Nyquist plots.

1. INTRODUCTION

Cathode material is one of the key components in lithium secondary battery and significantly affects its energy and power density [1-4]. So far, $LiCoO_2$, $LiFePO_4$, $LiMn_2O_4$, $Li(Ni_{1/3}Co_{1/3}Mn_{1/3})O_2$ are widely used in commercial LIBs. However, their theoretical capacities all below 200 $mAh \cdot g^{-1}$ and is far from meeting the growing demand of high performance lithium secondary battery with high energy density [2].

Molybdenum trioxide (MoO_3) is an attractive example of prospective cathode material for lithium secondary battery with high capacity. In general it exists in three different polymorphs, namely, quadrature phase α-MoO_3, monoclinic β-MoO_3 and hexagonal h-MoO_3. Among them α-MoO_3 is the most thermodynamic stable phase while β-MoO_3 and h-MoO_3 are thermodynamic metastable phases and will convert to α-MoO_3 under certain conditions [5, 6]. α-MoO_3 consists of distortional [MoO_6] octahedral structure units, which connect with the common edge units along the [001] direction and connect with the sharing of oxygen atoms vertex along the[100] and [001] direction. Therefore, a layered structure is built in flat space and this structure grows extensionally to form paralleled layer structures. These layered lattice frameworks alternately appear a large number of tetrahedron and octahedral structural units. There are a lot of holes and channels inside the internal structural units, also among [MoO_6]s, which allows microscopic particles (atoms, molecules and ions) to move freely [7]. It is reported that α-MoO_3 is peculiarly easy to be lithium ionized and forming Li_xMoO_3 after lithiation [8]. Each α-MoO_3 unit can accommodate about 1.5 Li^+ and the corresponding capacity is up to 279 $mAh \cdot g^{-1}$ when the potential is higher than 1.5 V. The conductivity of electron and Li^+ inner Li_xMoO_3 is also high. Hence, α-MoO_3 is considered a potential cathode material for lithium secondary battery.

Attempts have been made to use pure α-MoO_3 as cathode material for lithium secondary battery. However, performance is not satisfied [5, 6]. Deeply works reveal that octahedral structure of internal [MoO_6] is damaged in the process of lithium ion embedding in and escaping from α-MoO_3, which makes the layer spacing of α-MoO_3 not uniform, leading to its low capacity retention ratio and poor cycling performance [9-12]. Improvements should be developed to enhance the electrochemical performance of α-MoO_3 cathode material. So far, some methods have been utilized, including (1) developing various morphologies [13-19], (2) importing versatile carbon to stabilize the major structure [20-24], and (3) doping elements or compounds to modify the main material structure and increase electronic conductivity [25-29].

Recently, we developed a simple hydrothermal route to synthesize α-MoO_3 nanobelt without any surfactant [18]. The as-prepared α-MoO_3 nanobelt exhibited apparently better electrochemical performance than α-MoO_3 bulk. In this work, α-MoO_3 nanobelt@CNTs composite was further synthesized from α-MoO_3 nanobelt reported before and commercial CNTs via a simple ultrasonic method. Electrochemical performance of α-MoO_3 nanobelt@CNTs composite was measured. AC impedance spectroscopy was investigated to explain the microscopic mechanism of Li^+ transportation through α-MoO_3 nanobelts@CNTs composite in the first discharge process.

2. EXPERIMENT

2.1 Synthesis of α-MoO_3 nanobelt@CNTs composite

α-MoO_3 nanobelt was synthesized via a simple hydrothermal method without any surfactant as reported [18]. To prepare α-MoO_3 nanobelt@CNTs composite, α-MoO_3 nanobelt was first dispersed into adequate amount of deionized water. CNTs pretreated by nitric acid (HNO_3, 65 wt%) was then slowly added into above suspension with ultrasonic stirring until the suspension turned to dark black

colloidal or pasty liquid. The mass ratio of α-MoO_3 and CNTs was 7:3. Afterward the colloidal liquid was transferred into an air-flowing oven and dried at 80 ^oC for 12 h to get dark black solid. Finally the solid was moved to a muffle furnace to be sintered at 350 ^oC for 4 h in air to obtain α-MoO_3@CNTs composite.

2.2 Characterizations

The phase and structure of as-prepared material was characterized by using X-ray diffraction (D/Max-3B, Rigaku, Japan). The general parameters of XRD test were Cu target, K_α ray, graphite monochromator, 35 kV (tube voltage), 30 mA (tube current) and 5° min^{-1} (scanning rate). The morphology of the product was characterized using scanning electron microscopy (SEM) (FE-SEM, JEOL, Japan).

2.3 Electrochemical tests

In electrochemical performance test, lithium metal was employed as reference electrode and auxiliary electrode and 1 mol L^{-1} $LiPF_6$/EC+DEC+DMC (1:1:1 , W/W/W, Guangzhou Tinci) was used as electrolyte. The cathode was configured by 70 wt% of active material, 15 wt% carbon black (Shenzhen BTR), 5 wt% graphite (battery level, Shanghai Shanshan) and 10 wt% of polyvinylidene fluoride binder (PVDF, HS910, Elf-Atochem). Galvanostatic test (constant current charge and discharge test) was executed on battery tester (ZXZ-ZB, Shenzhen Neware) using 2032 coin cell. Cyclic Voltammetry (CV) was carried out on the electrochemical workstation (CHI660D, Shanghai Chenhua) using three-electrode battery model. The voltage range was from 3.50 V to 1.50 V and the scanning rate was 0.5 mV s^{-1}. Electrochemical impedance spectroscopy (EIS) was obtained by electrochemical workstation (CHI660D, Shanghai Chenhua). The standing time was 10^3 s. The frequency range was from 10^5 Hz to 0.01 Hz.

3. RESULTS AND DISCUSSIONS

3.1 The structure and morphology of α-MoO_3 nanobelt and α-MoO_3 nanobelt@CNTs composite

Figure 1 shows the XRD patterns of (a) α-MoO_3 nanobelt and (b) α-MoO_3 nanobelt@CNTs composite. All peaks on Figure 1 (a) can be attributed to typical orthorhombic α-MoO_3 (JCPDS card no. 05-0508). Sharply strong peaks demonstrate well crystallinity of the sample. It is observed that with the addition of CNTs, the composite remains original orthohombic structure and anisotropy growth trend along (0k0) crystal plane as pure α-MoO_3, indicating the retention of layered structure (Figure 1 (b)). However, the intensity of diffraction peak decreases, which is attributed to CNTs addition. Since CNTs is a kind of amorphous carbon, addition of CNTs into α-MoO_3 nanobelt is possible to degrade crystallinity, resulting in the decrease of diffraction peak.

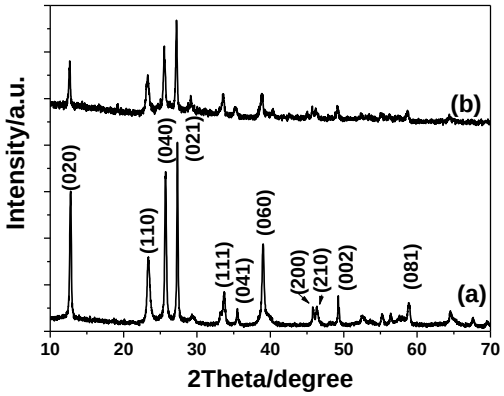

Figure 1. XRD pattern of (a) α-MoO_3 nanobelt and (b) α-MoO_3 nanobelt@CNTs composite.

Figure 2 shows the SEM images of (a) pure α-MoO_3 nanobelt and (b) α-MoO_3 nanobelt@CNTs. The α-MoO_3 nanobelt synthesized in our work all displays nanosized ribbon shape, indicating "nanobelt" feature of α-MoO_3. CNTs composition process makes the structure of α-MoO_3 nanobelt almost no change (Figure 2 (b)), except the disappearance of some small pieces (see white arrows on Figure 2 (a)). Meanwhile, most α-MoO_3 nanobelts are surrounded by CNTs, which may enhance the electronic conductivity α-MoO_3 nanobelt and improve the electrochemical performance.

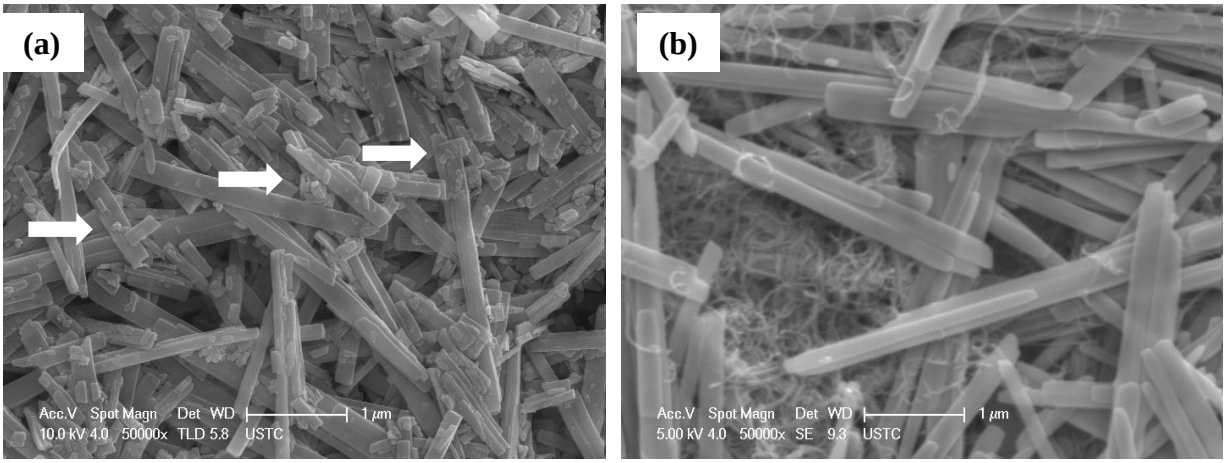

Figure 2. SEM images of (a) α-MoO_3 nanobelt and (b) α-MoO_3 nanobelt@CNTs.

3.2 Electrochemical characterization

Figure 3 (a-f) shows the charge-discharge profiles of α-MoO_3 nanobelt and α-MoO_3 nanobelt@CNTs composite in the potential range of 1.5-3.5 V at different C-rates. Figure 3(a) shows the typical charge-discharge curves of α-MoO_3, confirming the composition of α-MoO_3 of the as-prepared nanobelts. The first discharge curve exhibits two plateaus at about 2.7 and 2.2 V followed by a sloping region. The higher plateau at about 2.7 V disappears in the second cycle and is related to the

irreversible lithium ions de-intercalation from the MoO_6 octahedron intralayers, leading to the volume expansion of adjacent layer of MoO_6 octahedron [10, 11]. The lower plateau at about 2.2 V is related to the reversible lithium ion insertion/de-insertion in the interlayer lattice space [10] and is kept in subsequent cycles. However, after introducing CNTs to form α-MoO_3 nanobelt@CNTs composite (Figure 3(b)), both two discharge plateaus become shorter, resulting in a lower initial discharge capacity and indicating a negative influence on the initial discharge capacity of α-MoO_3 by introducing CNTs. Nevertheless, it is helpful to capacity retention. Table 1 summarizes the discharge capacity retention after 50 cycles for pure α-MoO_3 nanobelt and α-MoO_3 nanobelt@CNTs composite at a series of C-rates. Compared with pure α-MoO_3 nanobelt, the discharge capacity retention of α-MoO_3 nanobelt@CNTs composite at different C-rate is significantly improved from less than 50% to more than 60%. We attribute this improvement to the following three reasons: (1) Surrounding of α-MoO_3 nanobelt by CNTs not only improves the electronic conductivity of the whole composite, but weakens the volume change during Li intercalation/de-intercalation process as well. (2) Because of the inclination of the discharge plateaus in the first cycle after importing CNTs, it is inferred that CNTs partly inserts into the layer structure of α-MoO_3, occupies some parts of Li^+ channels or paths, and slows down the loss or attenuation of the capacity [23]. (3) After the addition of CNTs, some small pieces disappear and the morphology of α-MoO_3 nanobelt becomes more uniform (Figure 2). This might be helpful to the cyclic stability of α-MoO_3.

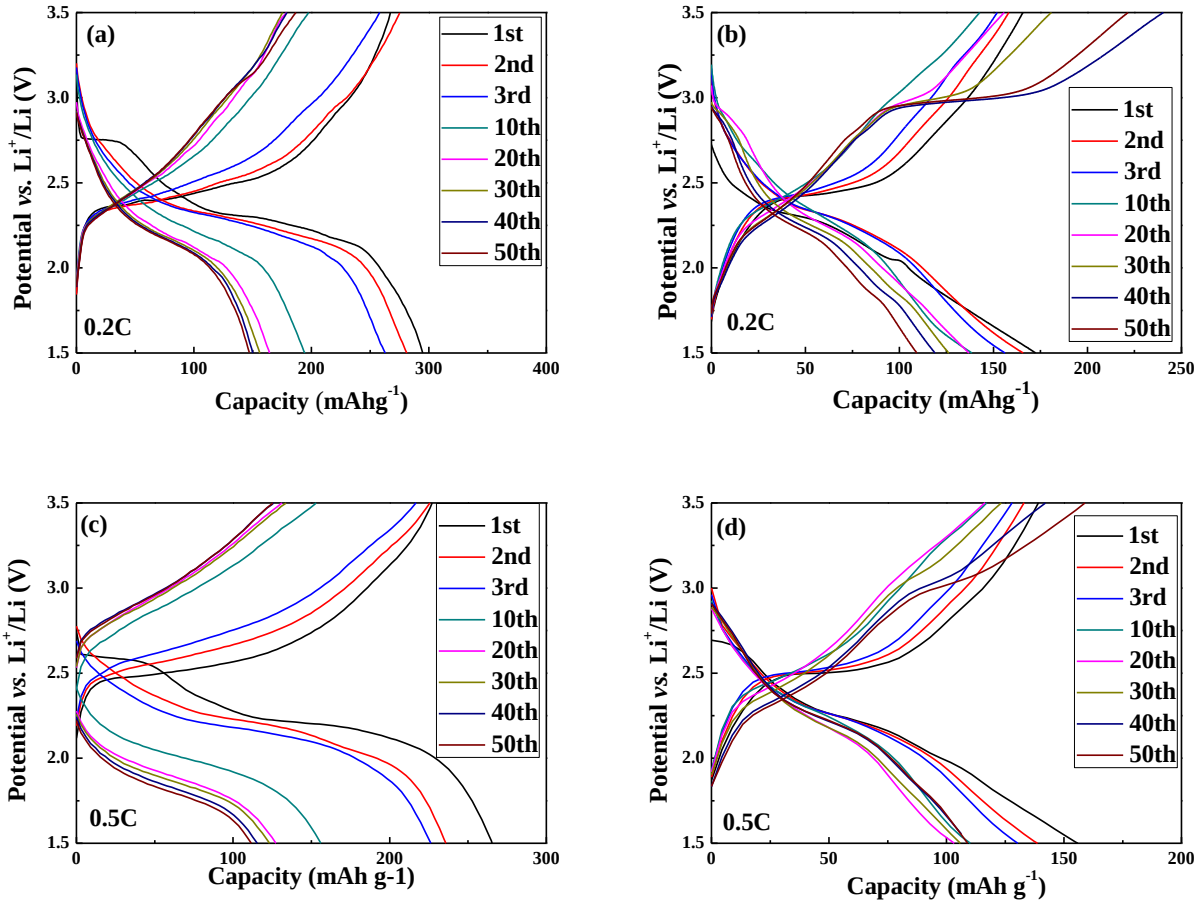

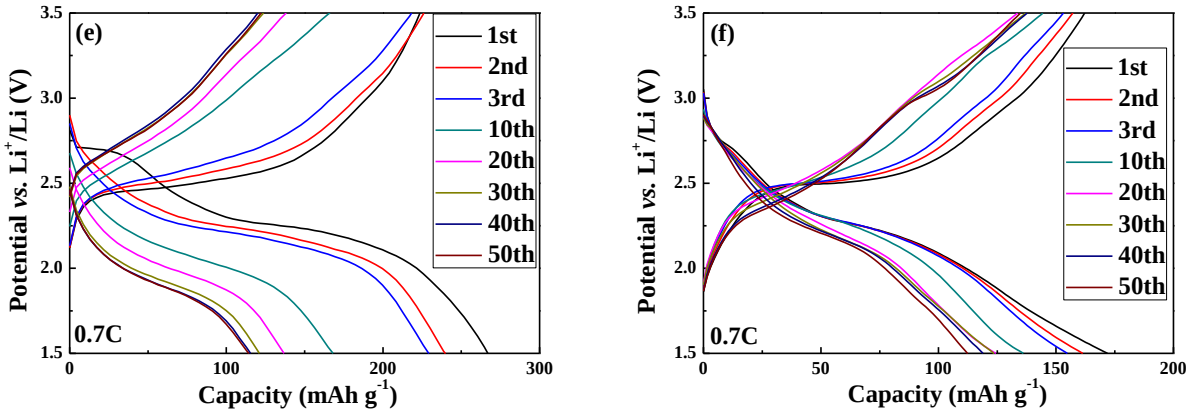

Figure 3. Charge-discharge curves of α-MoO_3 nanobelt (a, c, e) and α-MoO_3 nanobelt@CNTs composite (b, d, f) at 0.2C, 0.5C and 0.7C.

Table 1. Discharge capacity retention after 50 cycles for α-MoO_3 nanobelt and α-MoO_3 nanobelt@CNTs composite.

C- rate	α-MoO_3 nanobelt	α-MoO_3 nanobelt@CNTs composite
0.2C	49.91%	63.36%
0.5C	42.09%	69.83%
0.7C	42.84%	64.88%

Cyclic voltammetry (CV) measurement was examined to investigate electrochemical reaction of α-MoO_3 nanobelt and α-MoO_3 nanobelt@CNTs composite (Figure 4). Both cells were scanned for five cycles at 0.5 mV s^{-1}. CVs of α-MoO_3 nanobelt exhibits two pairs of oxidation and reduction peak at 3.07 V and 2.73 V, and 2.75 V and 2.24 V respectively, in the first cycle, which is in accord with literatures [17]. After composited with CNTs, the anodic peaks remain almost no change while the cathodic peaks shift to lower position, indicating a similar lithium insertion/extraction mechanism of α-MoO_3 nanobelt@CNTs composite to α-MoO_3 nanobelt. Besides these, a third reduction peak appears at 2.01 V in the first cycle, which might be attributed to the SEI formation reaction of CNTs. Similar phenomenon is also observed in the CV results of α-MoO_3/N-CNTs nanocomposite [24].

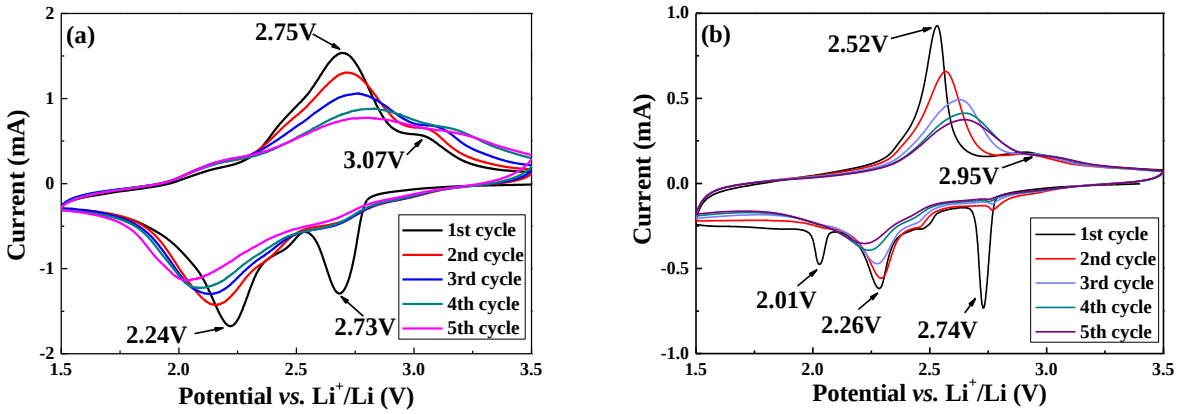

Figure 4. CV curves of (a) α-MoO_3 nanobelt and (b) α-MoO_3 nanobelt@CNTs composite for the first 5 cycles.

3.3 Impedance spectroscopy research of α-MoO_3/N-CNTs composite electrode in the first discharge process

In order to understand the electrochemical performance and the interface properties of α-MoO_3/N-CNTs nanocomposite, electrochemical impedance spectroscopy (EIS) was applied and the equivalent circuit was fitted.

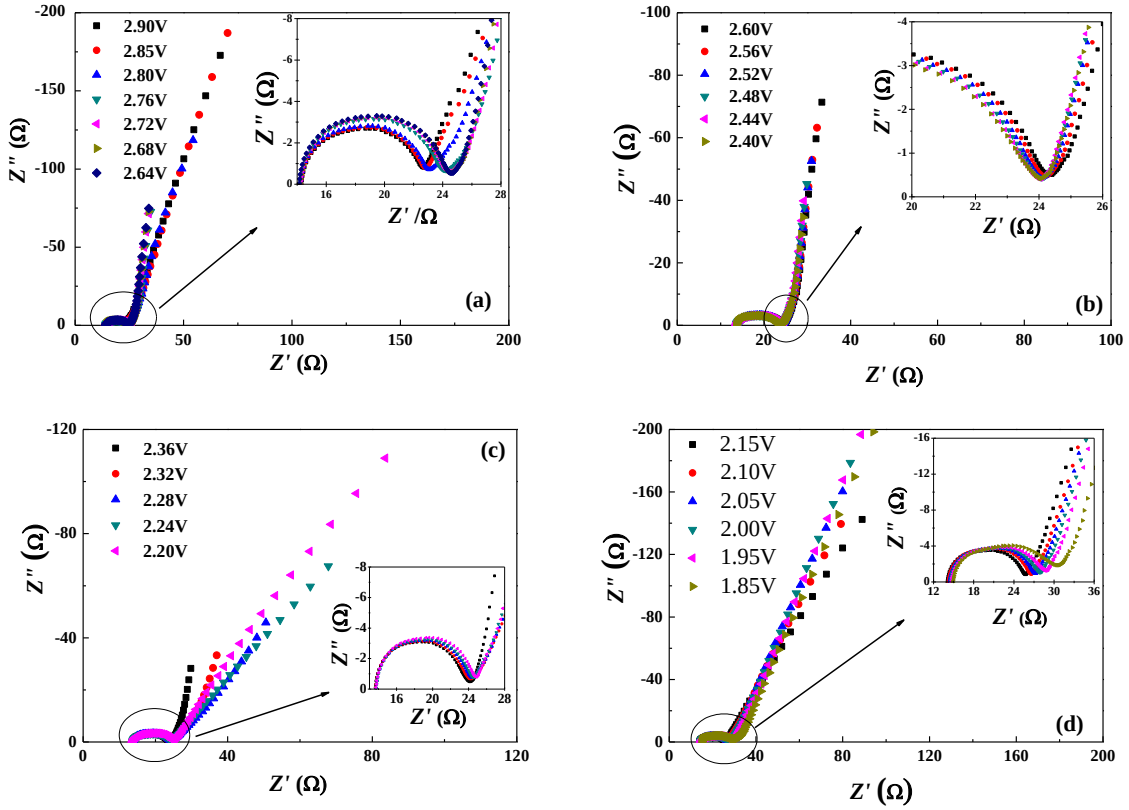

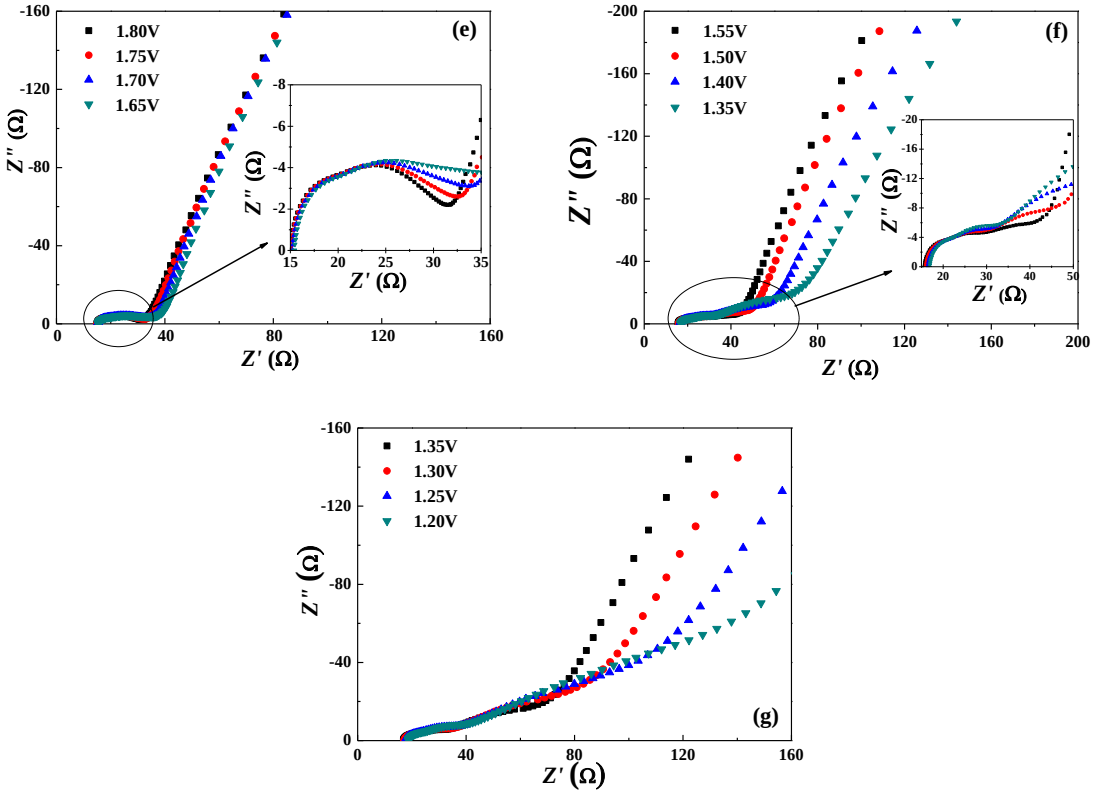

Figure 5. Nyquist plots of the α-MoO_3 nanobelts@CNTs composite electrode at various polarization potentials in the first discharge process: (a) 2.9-2.64 V; (b) 2.6-2.4 V; (c) 2.36-2.2 V; (d) 2.15-1.85 V; (e) 1.8-1.65 V; (f) 1.55-1.35 V and (g) 1.35-1.2 V.

Figure 5 shows the Nyquist plots of α-MoO_3 nanobelts@CNTs composite electrode at various polarization potentials in the first discharge process. When the polarization potential changed from 2.90 V to 1.65 V, Nyquist plots is composed of the high-frequency district of arc (HFA-a, 10^5-10^3 Hz), the high-frequency district of arc (HFA-b, 10^3-10 Hz) and the low-frequency district of slash (LFSL, 0.1-.001 Hz).

When the polarization potential continues to decrease to 1.55 V, except the above three parts, additional middle-frequency district arc (MFA, 10-0.1 Hz) is observed [30]. When the polarization potential further decreases to 1.2 V, there are some slight changes on three arcs and the gradient of low frequency slope which relates to the diffusion speed of Li^+ inside the electrode gradually declines.

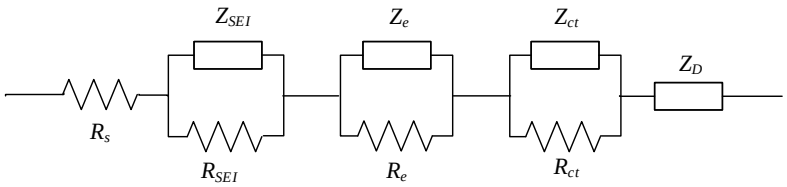

Figure 6. Equivalent circuit proposed for α-MoO_3 nanobelts@CNTs composite electrode in first discharge process.

Equivalent circuit is proposed for the analysis of α-MoO_3 nanobelts@CNTs composite electrode in the first discharge process (Figure 6). R_s, R_{SEI}, R_e and R_{ct} respectively represents ohm resistance, SEI film resistance, electronic-transfer resistance and charge-transfer resistance while constant phase element Z_{SEI}, Z_e, Z_{ct} and Z_D indicates diffusion impedance [30].

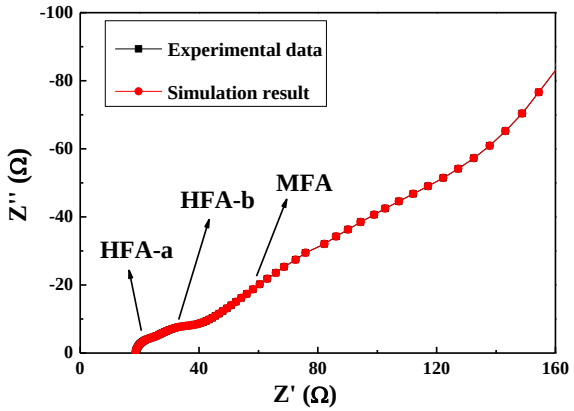

Figure 7. Comparison of Nyquist experimental data of α-MoO_3 nanobelts@CNTs composite electrode at 1.20 V and simulation result from equivalent circuit.

Figure 7 shows the comparison of experimental Nyquist data of α-MoO_3 nanobelts@CNTs composite electrode at 1.20 V and simulation result from equivalent circuit. Two lines are almost overlapped, indicating a high quality of simulation.

Figure 8 (a) shows variation of R_{SEI} with the polarization potential of α-MoO_3 nanobelts@CNTs composite electrode in the first discharge process. Apparently, R_{SEI} increases fast in the potential period of 2.9-2.7 V and 2.4-1.2 V. It is inferred that with the insertion of Li^+, the volume of α-MoO_3 particles is continuously expanding, resulting in the break of SEI layer on the surface and formation of new active surface [31]. This will lead to a new formation process of SEI layer and the whole SEI layer becomes thicker, resulting in the increase of R_{SEI}. Correlating R_{SEI} to CV and charge-discharge results, it is deduced that the increase of R_{SEI} in the period of 2.9-2.7 V lies on the process that Li^+ inserts inside the [MoO_6] space, while from 2.4-2.0 V, Li^+ inserts in the layers between [MoO_6] space group structure is responsible for the R_{SEI} growth.

Figure 8 (b) exhibits the variation of R_e with the polarization potentials of α-MoO_3 nanobelts@CNTs composite electrode in the first discharge process. Electronic conductivity of α-MoO_3 nanobelts@CNTs composite electrode is calculated by the formula $R=L/\sigma \cdot S$ and is of 10^{-4} S cm^{-1} at open circuit voltage. Kumagai et al reported that the electronic conductivity of pure α-MoO_3 was of 10^{-8} S cm^{-1} at room temperature [32]. Apparently, nanobelt morphology and CNTs addition improves the electronic conductivity dramatically. With the reducing of electrode potential, the resistance of the material gradually increases. It is found that α-MoO_3 is n-type semiconductor with 3.1 eV valence band [33-34] and owns similar electron conduction mechanism to single crystal $LiMn_2O_4$. From 3.5 to 1.2 V, α-MoO_3 follows an insertion/extraction mechanism with Li^+ and the major reaction could be expressed as follow:

$$x\mathrm{Li}^+ + x\mathrm{e}^- + \alpha\text{-}\mathrm{MoO_3} \rightleftharpoons \mathrm{Li}_x\mathrm{MoO_3} \quad (1)$$

Among them, x ($0 \le x \le 1.5$) represents Li^+ concentration. Li_xMoO_3 remains mixed-valence ($Mo^{6+}/Mo^{5+}/Mo^{4+}$) and its electronic conductivity mainly relies on the transition between the higher valence (Mo^{6+} and Mo^{5+}) and the lower valence (Mo^{5+} and Mo^{4+}). The conductivity is primarily controlled by the number of charge carriers from Mo^{6+} to Mo^{5+} and sequentially to Mo^{4+}, as well as the atomic distance of Mo-Mo [34].

When the discharge potential reaches 2.0 V, Mo^{5+} is almost transformed to Mo^{4+} [35]. The number of barriers decrease abruptly and the distance of Mo-Mo in orthorhombic structure is reduced, which may derive from the Coulombic force between Li^+ and the host [10]. There is an acceleration on R_e from 2.0 to 1.2V on Figure 8 (b). Therefore, it is concluded that the number of charge carriers is at least one of the key factors to the electronic conductivity of α-MoO_3.

Figure 8 (c) shows the variations of R_{ct} with the polarization potential of α-MoO_3 nanobelts@CNTs composite electrode in the first discharge process. When the electrode is discharged to lower than 1.55 V, additional middle-frequency district arc (MFA, 10-0.1 Hz) starts to be observed, indicating the emergence of $R_{ct.}$ However, R_{ct} is kept at a low value at the beginning, possibly due to the matter of electrode between conductor and semiconductor, with an excellent electronic conductivity. After discharged to 1.4 V, R_{ct} climbs up sharply, primarily caused by the re-generation of Li^+ enriched layer.

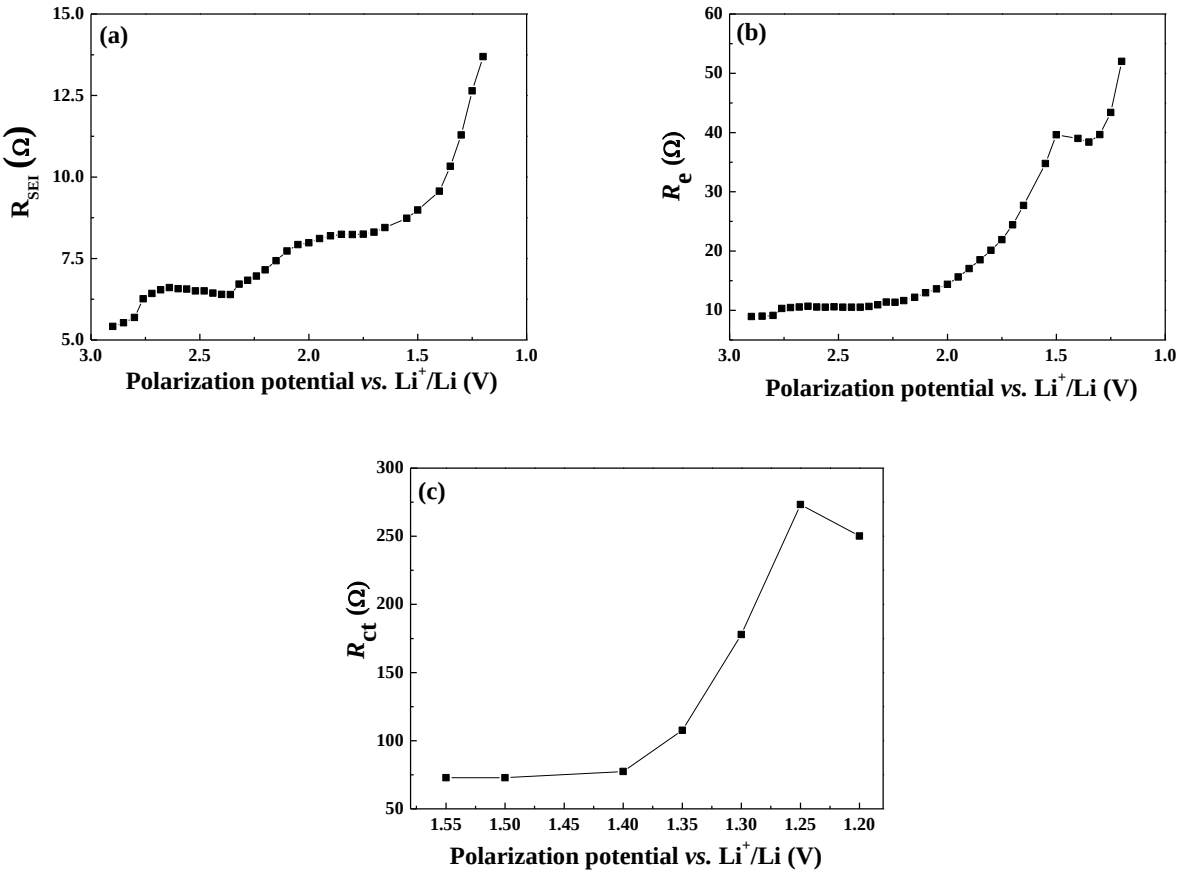

Figure 8. Variations of (a) $R_{SEI,}$ (b) R_e and (c) R_{ct} with polarization potentials of α-MoO_3 nanobelts@CNTs composite electrode in the first discharge process.

3.4 Discussion

CNTs is able to be winded on α-MoO_3 nanobelt very well, improving the density of the composite structure and reducing the volume expansion of α-MoO_3 nanobelt during charge-discharge process. Meanwhile, addition of CNTs could enhance the conductivity of α-MoO_3 composite and shorten the path for the transmission of electron. These benefit the electrochemical performance, especially the cycleability. Nevertheless, introducing CNTs will reduce the weight ratio of active material α-MoO_3 nanobelt in the whole cathode, thus lower the discharge capacity. An optimal amount of CNTs in α-MoO_3/CNTs composite needs to be further determined to balance the advantages and disadvantages of CNTs compositing.

EIS is a well-established technique to study electrode kinetics of electrode materials. It could offer information about the surface film, charge transfer and bulk resistances of the electrode, the associated capacitances and their variation with the applied voltage during the charge-discharge cycle [30]. It has been widely applied to explain the improvement on the electrochemical performance achieved by α-MoO_3 with various morphologies [13-17] or α-MoO_3 composite with carbon [20-24], polymer [25, 26] and inorganic compounds [27, 28]. In an earlier work, we have employed EIS technique to investigate the electronic and ionic transport properties of bulk α-MoO_3 as cathode material for rechargeable lithium battery [8]. In this work, the microscopic mechanism about the transport of Li^+ through α-MoO_3 nanobelt/CNTs composite is analyzed and explained in detail for the first time. Due to the nanosize feature of α-MoO_3 nanobelt which enhancing charge transfer, and the introductions of CNTs which forming SEI, solid electrolyte interface (SEI) resistance (R_{SEI}) starts to play a leading role at the beginning of the first discharge process (2.9-2.0 V), indicating a different feature to bulk α-MoO_3. Increased SEI resistance may be responsible for the lower discharge capacity of α-MoO_3 nanobelt/CNTs composite compared to α-MoO_3 nanobelt. In the following discharge process, electronic transmission resistance (R_e), and charge transfer resistance (R_{ct}), respectively plays an important role in different periods (2.0-1.5 V and 1.4-1.2 V) when Li^+ intercalates into cathode material, similar to the results of bulk α-MoO_3.

4. CONCLUSIONS

α-MoO_3@CNTs composite is synthesized from pure α-MoO_3 nanobelt and multi-walled carbon nanotubes (CNTs) via ultrasonic mixing process. Orthorhombic structure and morphology of nanobelt α-MoO_3 winded by CNTs is confirmed by XRD and SEM measurement. α-MoO_3 nanobelt@CNTs composite delivers less initial discharge capacity than pure α-MoO_3 nanobelt, but better cycling performance due to the addition of CNTs into composite, which increases the electronic conductivity and reduces the volume expansion. Microscopic mechanism of Li^+ transportation through α-MoO_3 nanobelt@CNTs composite electrode is revealed by cyclic voltammetry (CV) and electrochemical impedance spectroscopy (EIS). Nyquist plots of α-MoO_3 nanobelts@CNTs composite electrode *vs.* polarization potentials in the first discharge process show that during Li^+ intercalates into α-MoO_3 nanobelts@CNTs composite electrode, SEI-film resistance (R_{SEI}), electronic transmission resistance (R_e), and charge transfer resistance (R_{ct}) play an important role in different periods, respectively.

References

1. B. L. Ellis, K. T. Lee, L. F. Nazar, *Chem. Mater*., 22 (2010) 691.
2. M. S. Whittingham, *Chem. Rev*., 114 (2014) 11414.
3. R. Chen, T. Zhao, X. Zhang, L. Li, F. Wu, *Nanoscale Horiz*., 1 (2016) 423.
4. W. Li, B. Song, A. Manthiram, *Chem. Soc. Rev*., 46 (2017) 3006.
5. N. A. Chernova, M. Roppolo, A. C. Dillon, M. S. Whittingham, *J. Mater. Chem*., 19 (2009): 2526.
6. X. Hu, W. Zhang, X. Liu, Y. Mei, Y. Huang, *Chem. Soc. Rev*., 44 (2015) 2376.
7. L. Mai, B. Hu, W. Chen, Y. Qi, C. Lao, R. Yang, Y. Dai, Z. Wang, *Adv. Mater*., 19 (2007) 3712.
8. W. Bao, Q. Zhuang, S. Xu, Y. Cui, Y. Shi, Y. Qiang, *Ionics*, 19 (2013) 1005.
9. E. Hatzikraniotis, I. Samaras, K. M. Paraskevopoulos, C. Julien, *Ionics*, 2 (1996) 24.
10. T. Tsumura, M. Inagaki, *Solid State Ionics*, 104 (1997) 183.
11. Y. Iriyama, T. Abe, M. Inaba, Z. Ogumi, *Solid State Ionics*, 135 (2000) 95.
12. F. Leroux, L. F. Nazar, *Solid State Ionics*, 133 (2000) 37.
13. S. Berthumeyrie, J.-C. Badot, J.-P. Pereira-Ramos, O. Dubrunfaut, S. Bach, Ph. Vermaut, *J. Phys. Chem.*, 114 (2010) 19803.
14. L. Zhou, L. Yang, P. Yuan, J. Zou, Y. Wu, C. Yu, *J. Phys. Chem.*, 114 (2010) 21868.
15. U. K. Sen, S. Mitra, *RSC Adv.*, 2 (2012) 11123.
16. R. Nadimichela, W. Chen, X. Guo, *Mater. Res. Bull.*, 66 (2015) 140.
17. B. Han, K.-H. Lee, Y.-W. Lee, S.-J. Kim, H.-C. Park, B.-M. Hwang, D.-H. Kwak, K.-W. Park, *Int. J. Electrochem. Sci*., 10 (2015) 4232.
18. Y. Cui, Y. Pu, Y. Hao, Q. Zhuang, *Russ. J. Electrochem.*, 51 (2015) 119.
19. J. Li, S. Wei, G. Zhang, L. Xu, W. Li, K. Pan, *Int. J. Electrochem. Sci*., 12 (2017) 2429.
20. L. Noerochim, J.-Z. Wang, D. Wexler, Z. Chao, H.-K. Liu, *J. Power Sources*, 228 (2013) 198.
21. Y. Dong, S. Li, H. Xu, M. Yan, X. Xu, X. Tian, Q. Liu, L. Mai, *Phys. Chem. Chem. Phys*., 15 (2013) 17165.
22. B. Mendoza-Sánchz, P. S. Grant, *Electrochim. Acta*, 98 (2013) 294.
23. G. Wang, J. Ni, H. Wang, L. Gao, *J. Mater. Chem.* A, 1 (2013) 4112.
24. H. Zhang, X. Liu, R. Wang, R. Mi, S. Li, Y. Cui, Y. Deng, J. Mei, H. Liu, *J. Power Sources*, 274 (2015) 1063.
25. X. Wei, L. Jiao, J. Sun, S. Liu, H. Yuan, J. Solid State Electrochem., 14 (2010) 197.
26. V. M. Mohan, W. Chen, K. Murakami, *Mater. Res. Bull.*, 48 (2013) 603.
27. X. Wei, L. Jiao, S. Liu, J. Sun, W. Peng, H. Gao, Y. Si, H. Yuan, *J. Alloy Compd.*, 486 (2009) 672.
28. P. Cui, Y. Liang, Y. Sun, *Chin. J. Inorg. Chem*., 28 (2012) 1861.
29. D. P.Opra, S. V. gnedenkov, A. A. Sokolov, A. B. Podgorbunsky, N. M. Laptash, S. L. Sinebrukhov, *Mater. Lett*., 160 (2015) 175.
30. Q. Zhuang, S. Xu, X. Qiu, Y. Cui, L. Fang, S. Sun, *Prog. in Chem*., 22 (2010) 1044.
31. S. Mitra, P. Poizot, A. Finke, J.-M. Tarascon, *Adv. Funct. Mater*., 16 (2006) 2281.
32. N. Kumagai, N. Kumagai, K. Tanno, *J. Appl. Electrochem*., 18 (1988) 857.
33. I. G. Austin, N. F. Mott, *Adv. Solid State Phys*., 9 (1969) 22.
34. Y. S. Jung, S. Lee, D. Ahn, A. C. Dillon, S.-H. Lee, *J. Power Sources*, 188 (2009) 286.
35. S. M. Jolanta, D. D. Soline, *J. Phys. Chem.* C, 112 (2008) 11050.